EVOLUTION OF MAGMAS AND MAGMA SOURCES TO THE COAST MOUNTAINS BATHOLITH, BRITISH COLUMBIA, CANADA, REFELCTED BY ELEMENTAL AND ISOTOPIC GEOCHEMISTRY

by

James Daniel Girardi

A Thesis Submitted to the Faculty of the

DEPARTMENT OF GEOSCIENCES

In Partial Fulfillment of the Requirements
for the Degree of

MASTER OF SCIENCE

In the Graduate College
THE UNIVERSITY OF ARIZONA
2008

Evolution of magmas and magma sources to the Coast Mountains Batholith, British Columbia, Canada, reflected by elemental and isotopic geochemistry

James D. Girardi, P. Jonathan Patchett, Mihai N. Ducea, George E. Gehrels,
Department of Geosciences, University of Arizona, Tucson, AZ 85721
Margaret E. Rusmore,
Department of Geology, Occidental College, Los Angeles, CA 90041
Glenn J. Woodsworth,
Geological Survey of Canada, Vancouver, British Columbia V6B 5J3
David M. Pearson, and Christian Manthei,
Department of Geosciences, University of Arizona, Tucson, AZ 85721

Abstract

New Nd and Sr isotopic data from 80 plutonic rocks of the southern Coast Mountains Batholith (CMB) ranging in age from 198 - 50 Ma have overall primitive characteristics with initial ε_{Nd} ranging from -2 to +8 and initial $^{87}Sr/^{86}Sr$ ratios mainly in the range 0.7030 - 0.7050. These isotopic data vary with time and are strongly correlated with the patterns of rare-earth element (REE) abundance, particularly $(La/Yb)_N$ values. $(La/Yb)_N$ ranges from 5 – 65, with high $(La/Yb)_N$ corresponding to lower initial ε_{Nd} and higher initial $^{87}Sr/^{86}Sr$. Periods when $(La/Yb)_N$ was low and the isotopic ratios of Nd and Sr appear more mantle-like (140-120 Ma and 80-60 Ma) separate three periods (160-140 Ma, 120-80 Ma, and 58-50 Ma) when high $(La/Yb)_N$ was accompanied by less primitive Nd and Sr isotopic ratios. These geochemical episodes are strongly correlated with magmatic flux in the CMB, reflected by U-Pb zircon ages of all plutons analyzed (Gehrels et al., 2008). High $(La/Yb)_N$, low initial ε_{Nd}, and high initial $^{87}Sr/^{86}Sr$ correspond to high magmatic flux, with the opposite geochemical and isotopic signatures corresponding to low magmatic flux. The rare-earth element patterns have either no, or very weak Eu anomalies, regardless of age, rock type, or $(La/Yb)_N$ values. The lack of significant Eu anomalies firmly indicates that neither plagioclase crystal fractionation nor melting to leave plagioclase-bearing residues were important in production of the batholith, so that melting must have occurred below 40 km depth.

Steep REE patterns, expressed by high $(La/Yb)_N$ values, are interpreted as a result of fractionation induced by garnet-rich melting residues. High $(La/Yb)_N$ corresponds to deeper melting leaving garnet-rich residues, while low $(La/Yb)_N$ magmas were separated from garnet-poor residues at shallower depth. The correlation of high magmatic flux with low initial ε_{Nd}, high initial $^{87}Sr/^{86}Sr$, and high $(La/Yb)_N$ in the granitoids suggests a connection with underthrusting and overthickened crustal roots where there is an increased availability of partial melts from supracrustal lithologies, and the production of

garnet-rich residues. The results demonstrate a cyclic pattern where thickening, and the supply and extensive melting of supracrustal materials at depth to leave garnet-rich residues, were punctuated by two periods when melting was less intense and shallower, magmas became isotopically more primitive, and garnet-poor residues were produced. In turn, these cyclic patterns suggest a tectonic model where high magmatic flux fueled by crustal thickening and enhanced lower crustal melting is followed by lithospheric thinning due to the loss of garnet-rich batholithic roots via delamination or foundering which occur during low magmatic flux. Delamination or foundering events create the space for renewed rapid crustal thickening and sets the stage for the next high magmatic flux and batholithic root forming episode.

Introduction

The Coast Mountains Batholith (CMB), also referred to as the Coast Plutonic Complex) constitutes one of the worlds largest batholithic suites generated from predominately mantle sources beneath a continental magmatic arc. The CMB can be traced from northern Washington continuously for over 1700 km along the coast of western North America through British Columbia, southeast Alaska, and into southwestern Yukon (Roddick and Hutchinson, 1974; Gehrels et al., 2008) and represents the largest exposed batholithic complex in North America (Barker and Arth, 1984). Studies of the CMB have proved invaluable in our understanding of Canadian Cordilleran Tectonics (Armstrong, 1988; van der Heyden, 1992; Ghosh, 1995, Gehrels et al., 2008), and in the genesis of continental crust and crustal growth (Samson et al., 1991a; Samson and Patchett, 1991; Hollister and Andronicos, 2006).

Nd and Sr isotopic investigations of the CMB have established the predominantly juvenile nature of these arc rocks, which is best observed in southern British Columbia (Armstrong, 1988; Cui and Russell, 1995; Friedman et al., 1995). The presence of an ancient continental margin assemblage, indicated from predominately Proterozoic-aged zircons from metamorphic rocks and inheritance of Proterozoic-aged zircons in plutons of the west flank of the northern CMB (Gehrels et al., 1990), may perhaps explain the

more crustally evolved isotopic signatures of plutons in the northern CMB (Samson et al., 1991a, 1991b). The occurrence of primitive metamorphic country rocks, which are in some cases more juvenile isotopically than the CMB intrusives themselves (Patchett et al., 1998), suggest that the isotopic chemistry is controlled from deep in the crust, not by assimilation at shallow levels.

To date, magmagenesis depths and sources for the CMB have been somewhat poorly constrained; previous studies suggest these rocks are predominately mantle derived but may contain ~10 – 50 % recycled crustal material (Samson et al., 1991b; Cui and Russell, 1995). In addition, for granitoids in general, a range of processes have been proposed to modify magmas initially formed at the base of the crust (Hildreth and Moorbath, 1988), as they rise to the shallower depths of pluton emplacement. Intracrustal assimilation and fractional crystallization (AFC) (DePaolo, 1981) and crustal anatexis (Patino-Douce et al., 1990) may provide mechanisms for generating the gabbroic to granitic compositions and the primitive to more crustal isotopic signatures of plutonic rocks. Previous work by Ghosh and Lambert (1995) and Samson et al. (1991b), respectively, address these models for petrogenesis in the CMB.

In this study, new Nd and Sr isotopic, major and rare earth elemental data are reported for 80 plutonic rock samples. The samples lie in a restricted region of the south-central CMB, and represent three transects across the batholithic complex. The rocks sampled encompass Jurassic – Eocene magmatism in the CMB and span periods of terrane accretion, translation, and deformation as the western edge of northwest North America was formed (Armstrong, 1988; Monger and Price, 2002). The approach of this study is to comprehensively characterize the elemental and isotopic chemistry of the

sample suite, and to develop constraints on petrogenesis and tectonic processes in the Cordilleran magmatic arc.

Tectonic Setting

The CMB represents a volumetrically substantial part of the Coast Mountains orogen and mainly lies between the allochthonous Alexander-Wrangellia composite terrane to the west, and the Stikine terrane to the east (Jones et al., 1977; Samson et al., 1991b; Gehrels et al., 2008) (Figure 1). Early to mid-Jurassic magmatism in these terranes presently bounds the CMB to the east and west (Gehrels et al., 2000, 2008) and was generated under relatively direct convergence (Engebretson et al., 1985). Subsequently, the mid-late Cretaceous closing of the Gravina Basin (Monger et al., 1982; Brew et al., 1992) juxtaposed Alexander-Wrangellia to southern Yukon-Tanana and northern Stikine. Following the final accretion of the Alexander-Wrangellia terrane to inboard terranes during mid-Cretaceous time (ca. 100 Ma) (Monger et al., 1982, Crawford et al., 1987; Armstrong, 1988), sinistral translation along the continental margin is interpreted to have ultimately led this crustal fragment, once the northern continuation of the Jurassic arc which also intrudes the Stikine terrane (now eastern portion of CMB), to become the western portion of the CMB (Monger et al., 1994; Gehrels et al., 2008).

In contrast to the earliest stages of batholith development, the 88 Ma and younger plutons which make up most of the CMB by mass (Crawford et al., 1997; Hollister and Andronicos, 2006) were generated after terrane accretion and under dextral oblique convergence as terranes translated northward (Andronicos et al., 1999; Hollister and

Andronicos, 2000). Studies of the northern CMB have shown that 58 – 50 Ma plutons are distinct from other pre- and post- terrane accretion intrusives in that they were emplaced into the arc during orogenic collapse under highly dextral oblique convergence (Hollister and Andronicos, 2006). As a result of orogenic collapse, the present surface exposures of the voluminous plutons which dominate the exposed rock record are possible due to deep levels of crustal exhumation (Hollister, 1982; Rusmore et al., 2005).

The study area (Figure 1) and the northern CMB in southernmost southeast Alaska have been studied as part of both the ACCRETE and BATHOLITHS multidisciplinary projects. A comprehensive review of previous work is presented in Gehrels et al. (2008), who also present U-Pb zircon ages for all the plutons included in the present study. The age data yield a magmatic production curve for the study region, showing periods of high and low production, which are instrumental for our interpretations. The geology shown in Figure 1 is modified from Rusmore et al. (2005), and shows the major tectonostratigraphic units and major Tertiary faults. The Coast Shear Zone (thick black line) is an important feature that parallels the Coast Mountains orogen and has accommodated thrust, normal, and strike-slip motion (Brew and Ford, 1978; Ingram and Hutton, 1994; Klepeis et al, 1998). Samples for this study were collected along three main transects across the arc, indicated by boxes in Figure 1 as: A, Douglas Channel in the north; B, Mathieson Channel in a central position; and C, the Burke/Dean Channels to the south.

Results

Major and Rare Earth Element Geochemistry

All CMB samples in this study were analyzed for their major element compositions at Macalester College using X-ray fluorescence spectrometry, and for their rare earth element compositions at the University of Saskatchewan using inductively coupled plasma mass spectrometry (Table 1). The CMB samples are intermediate (average 65% SiO_2), and mainly of dioritic-tonalitic bulk composition. At silica <70 wt% the rocks are calc-alkalic, but for the few samples >70 wt% SiO_2 there is a change to alkali-calcic compositions according to the modified alkali-lime index of Frost et al. (2001). Samples are also predominantly metaluminous, with alumina saturation index (ASI) ranging from 0.71 – 1.19. Weak to moderately peraluminous (ASI 1 to 1.1) and strongly peraluminous (ASI >1.1) represent a small population of samples which have bulk compositions with >70% SiO_2. Harker diagrams (Figure 2) show that K_2O increases while TiO_2, total Fe as Fe_2O_3, and Na_2O decrease with increasing silica content. As noted by Driver et al. (2000) trends of this nature may represent either fractional crystallization or mixing of magmas from different sources.

Chondrite-normalized (Anders and Grevesse, 1989) rare earth element (REE) patterns for selected samples, formed during high and low flux magmatism respectively, are shown in Figure 3. These samples, which are representative of CMB rocks in this study, show varying degrees of heavy REE (HREE) depletion, and accordingly display moderate to steeply dipping REE patterns. All samples lack significant Eu anomalies, shown by average Eu/Eu* (Table 1) only slightly less than unity (0.92). La/Yb chondrite-normalized ratios ($(La/Yb)_N$) backed by U-Pb zircon ages (Gehrels et al., 2008) are also shown in Table 1 and are plotted in Figure 4 as a function of time and magmatic flux. In Figure 4 the black out-lines separate three periods, 200 – 140 Ma, 140 – 80 Ma,

and 80 – 50 Ma, for which increasing $(La/Yb)_N$ ratios are seen. Each of these periods begins with low $(La/Yb)_N$ ratios (≤10) and increases to values of 20 to 65. These differing $(La/Yb)_N$ ratios correspond exactly to the two distinct populations of REE patterns shown in Figure 3. The increasing $(La/Yb)_N$ ratios, especially in the last 10 My of each period, are interpreted below to indicate that very different residual mineral assemblages are forming throughout the construction of the CMB.

Nd and Sr Isotopic Geochemistry

Nd and Sr isotopic results, backed by U-Pb zircon ages (Gehrels et al., 2008), are shown in Table 2 and are plotted in Figures 5 and 6 as a function of time and magmatic flux. Nd and Sr analytical methods follow Patchett and Ruiz (1987). The isotopic data of this study and work done farther to the south (Cui and Russell, 1995; Friedman et al., 1995) are in agreement with the well established isotopically primitive nature of the southern CMB compared to the more crustally evolved signatures observed in the northern CMB (Samson et al., 1991b), and also to the east of the CMB (Ghosh, 1995; Ghosh and Lambert, 1995). Both the Nd and Sr isotopic data reveal three distinct time periods during the construction of the CMB which are characterized by steady trends to isotopically less primitive signatures (lower ε_{Nd}, higher $^{87}Sr/^{86}Sr$) with intervening abrupt excursions to more primitive isotopic signatures (higher ε_{Nd}, lower $^{87}Sr/^{86}Sr$). Fluctuations between more and less primitive isotopic signatures are interpreted below to reflect a reoccurring tectonic process controlling the proportion of mantle to crustal magmatic contributions to CMB magmas.

During the period 200 – 140 Ma both the western and eastern Jurassic – Early Cretaceous arcs show trends to less primitive isotopic signatures with decreasing initial

ε_{Nd} and increasing initial $^{87}Sr/^{86}Sr$. The eastern Jurassic arc (solid triangles) was active in the Stikine terrane and shows a restricted range of primitive signatures with initial ε_{Nd} decreasing from +7.7 to +6 and initial $^{87}Sr/^{86}Sr$ increasing from 0.7030 to 0.7035 in samples ranging in age from 182 – 145 Ma. In contrast the western Jurassic arc (open squares) which intrude the Alexander-Wrangellia terrane show a more variable range with initial ε_{Nd} decreasing from +6 to -2 and initial $^{87}Sr/^{86}Sr$ increasing from 0.7035 to 0.7055 in samples ranging in age from 198 – 145 Ma. Differences between the isotopic characteristics of the eastern and western Jurassic arcs are inferred to be due to their different tectonic settings during the Jurassic (Monger, 1994; Gehrels et al., 2008). An abrupt change to more isotopically primitive characteristics is apparent in the sparse samples that range in age from 140 – 120 Ma. Isotopic values steadily change from this point forward and an especially well defined trend to less primitive isotopic signatures is clear from 108 – 80 Ma. During this time initial ε_{Nd} decreased from +7 to +3 and initial $^{87}Sr/^{86}Sr$ increased from 0.7035 to 0.7047.

The period between 80 and 70 Ma marks another abrupt change to isotopically primitive signatures, with initial ε_{Nd} increasing to +7 and initial $^{87}Sr/^{86}Sr$ decreasing to 0.7033 by 70 Ma. A return to isotopically less primitive signatures occurred during 70 – 50 Ma with initial ε_{Nd} decreasing to +4 and initial $^{87}Sr/^{86}Sr$ increasing to 0.7040 by 50 Ma in samples collected from the Douglas Channel (Transect A, Figure 1). Along the Mathieson Channel and Burke/Dean Channel transects (B and C, respectively, Figure 1) significantly more crustal isotopic signatures are observed with initial ε_{Nd} decreasing to -2 and initial $^{87}Sr/^{86}Sr$ increasing to 0.7060 from 58 – 50 Ma. From these observations it is clear that the period 200 – 50 Ma is characterized by fluctuations between trends

towards more crustal isotopic signatures and abrupt changes to primitive isotopic signatures. Inflection points between trends of decreasing initial ε_{Nd} and increasing initial $^{87}Sr/^{86}Sr$ (evolving towards more crustal) and increasing initial ε_{Nd} and decreasing initial $^{87}Sr/^{86}Sr$ (more primitive) occur around ~140, 80 and 70 Ma (Figures 5 and 6).

Discussion

Primitive isotopic signatures (high ε_{Nd}, low $^{87}Sr/^{86}Sr$) from the majority of plutonic rocks analyzed in this study confirm the generally juvenile nature of the southern CMB (Cui and Russell, 1995; Friedman et al., 1995; Patchett et al., 1998). However, it is significant that the Nd and Sr isotopic characteristics and $(La/Yb)_N$ of rocks in this study show a systematic correlation with age, which contrasts other studies of the CMB (with the exception of Armstrong's (1988) seminal work) that have found no correlation of isotopic characteristics with age, rock type, or distance along the study transect. This discussion will address the constraints Nd and Sr isotopic systems and $(La/Yb)_N$ ratios place on magmagenesis in the CMB, and focus on constraints which the exposed geology places on mechanisms that can explain the correlations between the data and magmatic flux.

During 120 – 80 Ma high magmatic flux, an increasing crustal magma component, and increased residual garnet stability are followed by the opposite trends during 80 – 70 Ma. The very well constrained geologic history in the CMB and clearly defined fluctuation in magmatic flux, isotopic and geochemical trends (Figures 4,5, and 6), makes 100 – 70 Ma a well suited base to build well constrained tectonic models explaining what governs magmatic flux and magma sources in continental magmatic

arcs. It will be shown that it is important to distinguish between pre-terrane accretion (>100 Ma) and post-terrane accretion (<100 Ma) tectonic configurations in the CMB. First mechanisms which induce and sustain high flux magmatism will be investigated, followed by probing the transition to low flux magmatism. Tectonic models developed for geologically well constrained Mid to Late Cretaceous will be used to then assess Mid to Late Jurassic high flux magmatism, for which the geologic history is less well constrained, and Eocene high flux magmatism, which has a more complicated geologic history.

Constraints from REE patterns

Two features of the REE patterns are very important for discussion of petrogenetic models for the CMB: their lack of significant Eu anomalies and variation in the degree of heavy REE depletion (Table 1, Figure 3). Because plagioclase fractionates Eu with a crystal/liquid distribution coefficient around 2 for magmatic redox conditions (Weill and Drake, 1973), then magmas must carry a negative Eu anomaly (Eu/Eu*<1) if they were affected either by equilibration with significant plagioclase residues or removal of significant plagioclase crystal fractionates. In comparison to typical upper continental crustal Eu/Eu* of ~0.65 (Taylor and McLennan, 1985), the CMB samples of this study have average Eu/Eu* of 0.92, and many samples show no negative anomaly at all (Table 1, Fig. 3). This means that the magmas must have generally been produced below the level of plagioclase stability (~40 km), and have not undergone a large degree of crystal fractionation in the crust, because magmatic compositions like those in the CMB would be in equilibrium with large amounts of plagioclase at depths less than 40 km.

The second powerful constraint comes from the steepness of the REE pattern, expressed by $(La/Yb)_N$ ratios. It is evident from Figure 3 that the difference between the two groups of REE patterns is not mainly light REE enrichment, but heavy REE (HREE) depletion. It seems overwhelmingly likely that HREE have been removed or held back from the magma during melting. Although amphibole and pyroxene in large abundance can affect HREE, it is garnet which has partition coefficients for HREE that can be 100 times those of any other major rock-forming mineral (e.g. Taylor and McLennan, 1985) that is most effective. It seems a natural conclusion that garnet, whose stability increases with depth in almost all rock compositions, is the residual mineral which has caused the HREE depletion of CMB magmas.

The lack of Eu anomalies and HREE depletion in the plutonic rocks of this study indicates that low pressure anatexis (Gerbi, 2006), or melts formed during orogenesis in the absence of heat transfer by mantle-derived melts (England and Thompson, 1986) are not significant contributors to magmatism. Rather it is more likely that the effects of basaltic underplating at the base of the crust promote the partial melting and incorporation of lower crustal amphibolite – granulite lithologies (Hildreth and Moorbath, 1988; Dufek and Bergantz, 2005; Hollister and Andronicos, 2006). On this basis, the relationship of high magmatic flux to HREE depletion, and the lack of HREE depletion when the magmatic flux was lower (Fig. 4), means that garnet was a dominant residual mineral only during the times of high magmatic flux during 160-140 Ma, 120-80 Ma and 58-50 Ma. Intervening periods (140-120 and 80-60 Ma) are inferred to have melting that was both less intense and shallower, and also at these times garnet was much less significant as a residual phase.

Correlation of Nd, Sr isotopes and REE with Magmatic Flux

The relationships between $(La/Yb)_N$, Nd and Sr isotopes, and magmatic flux are in general simple, with higher ε_{Nd} and lower $^{87}Sr/^{86}Sr$ corresponding to higher $(La/Yb)_N$ and high magmatic flux, which occurs during 160-140 Ma, 120-80 Ma and 58-50 Ma, after which arc magmatism in the CMB ceased. Intervening periods from 140-120 Ma and 80-60 Ma show the inverse set of correlations. The interpretation of HREE depletion as indicating formation of garnet-rich melting residues allows a straightforward sequence of tectonic/petrogenetic environments to be established.

Periods of low flux magmatism from 200 – 160 Ma, 140 – 120 Ma, and 80 – 60 Ma are characterized by primitive signatures (initial ε_{Nd} commonly > +4 and initial $^{87}Sr/^{86}Sr < 0.7040$) with garnet-poor residual assemblages ($(La/Yb)_N \leq 10$). On the other hand, periods of high flux magmatism, 160-140 Ma, 120 – 80 Ma, and 58 – 50 Ma are characterized by more crustally evolved signatures (initial ε_{Nd} commonly <+4 and initial $^{87}Sr/^{86}Sr > 0.7040$) with garnet-rich residual assemblages ($(La/Yb)_N = 30 – 65$). Nd and Sr isotopes indicate that there was an increased crustal contribution to magmas generated during periods of high magmatic flux, while periods of low magmatic flux are dominated by a primarily mantle magma source. These opposing relations indicate that the proportion of crustal to mantle magma components is dramatically different between periods of high and low magmatic flux.

Cyclic formation of Dense Igneous Residues

Figure 7 is a comparison of chondrite-normalized REE patterns from selected CMB samples of this study (Figure 3) and average REE plots for rocks exposed at the surface of the central Sierra Nevada Batholith (CSNB) (Dodge et al, 1982). Similarities

between the chondrite-normalized REE patterns from the CMB and the CSNB shown in Figure 7 are significant since there has been direct xenolith evidence in the CSNB for the formation of dense garnet rich (~50%) residual assemblages (Ducea, 2002). This evidence supports the formation of dense garnet-rich residual assemblages in the CMB during times of high $(La/Yb)_N$ and steep REE patterns (Figures 3 and 4). The cyclic change in $(La/Yb)_N$ shown in Figure 4 also correlates with magmatic flux, indicating that periods of high magmatic flux are characterized by high $(La/Yb)_N$, thicker crust and dense garnet-rich residues, whereas periods of low magmatic flux are characterized by low $(La/Yb)_N$, shallower depths of magmagenesis, and garnet poor residues. The repetition of the patterns through time argues strongly that these processes are part of a tectonic cycle that governs magmatism in this continental arc.

Geologic Constraints

There are many important geologic constraints which can place controls over viable mechanisms that may explain the correlated trends in magmatic flux, Nd and Sr isotopes, and $(La/Yb)_N$ in the CMB during 200 – 50 Ma. First order constraints come from plate tectonic reconstructions (Engebretson et al., 1985) which place control over plate motions and possible stress states that may have existed in the upperplate. Second order constraints arise from the timing relations determined among the deformational and metamorphic events which reveal detailed information of stress and thermal states in the upperplate (summarized in Gehrels et al., 2008). Finally, third order constraints come from the plutonic rock record, which may provide both robust age constraints and details such as: the rate, location, and direction of magmatism; potential magma sources;

magmatic flux; and geochemical evidence for depths of magmagenesis and the magnitude of residual garnet stability.

The geologic history during 100 – 80 Ma is very well documented and allows a robust investigation into the mechanisms which fueled high flux magmatism and the isotopic and geochemical trends observed during this time. In contrast, there are considerable uncertainties in the tectonic history of the outboard Alexander-Wrangellia terrane and in the opening and closing of the Gravina Basin between 160 to 100 Ma (summarized in Kapp and Gehrels (1998)) which prevent a straightforward explanation of the magmatic flux for this time. Although the geologic history surrounding the final Eocene high flux magmatic event is well documented (Andronicos et al., 2003; Rusmore et al., 2005; Hollister and Andronicos, 2006), it is considerably more complicated than earlier high flux magmatic episodes since it was intimately related to the collapse of the arc. The period 100 – 80 Ma is thus the best time period to begin to probe the mechanisms of which may govern high magmatic flux in the CMB, and to explain the observed isotopic and geochemical trends.

One way to view the isotopic and geochemical trends, which indicate increasingly garnet-rich igneous residues and more crustally evolved isotopic signatures during high flux magmatism during 100 – 80 Ma (Figures 4, 5, and 6), may be to consider a tectonic process shared among these features observed in the data. Crustal shortening is a mechanism that has been proposed to trigger magmatic flare-ups in the U.S. Cordillera (Ducea, 2001; Ducea and Barton, 2007); this may be a viable mechanism to explain high flux magmatism in the CMB since there is well documented crustal deformation associated with the accretion of the Alexander-Wrangellia composite terrane thus

satisfying a first order constraint that there were convergent tectonics (necessary for crustal shortening) during this period (Engebretson, 1985).

Second order geologic constraints are also derived from timing relations among documented crustal shortening styles, vergence, and episodes (Monger, 1982; Coney and Jones, 1985; Crawford et al., 1987; Rubin et al., 1990). Third order constraints arise since crustal shortening and thickening are mechanisms that can explain deeper levels of magmagenesis which would increase residual garnet stability and $(La/Yb)_N$ (Kay et al., 2005) and also promote the incorporation of crustal materials into the magma source (Patino-Douce et al., 1990), and may explain trends to less primitive isotopic signatures and increased magmatic flux during 100 – 80 Ma (Figures 4, 5, and 6). It is a significant geologic constraint that following the 100 – 90 Ma episode of thrusting and crustal shortening associated the convergence of the Alexander-Wrangellia and Stikine-Yukon Tanana Terrane superterranes through ~85 Ma (Rubin et al, 1990) trends to evolving Nd and Sr isotopic signatures and a steady rise in $(La/Yb)_N$ occur during increasing magmatic flux (Figures 4, 5, and 6).

Following the mid-Cretaceous accretion of the Alexander-Wrangellia terrane, maximum $(La/Yb)_N$ (Fig. 4) was attained in rocks sampled from the Burke/Dean Channel (Transect C, Figure 1). The greater $(La/Yb)_N$ is attributed to increased garnet stability due to deeper levels of magmagenesis and thicker crust (Rapp and Watson, 1995; Kay et al., 2005), and suggests these conditions existed in the southern portion of the study area along the Burk/Dean Channels compared to the northern study area along the Douglas Channel (Figure 1) . $(La/Yb)_N$ values which are predominately < 10, and primitive isotopic signatures prevail between 120 – 100 Ma (Figures 4, 5, and 6) suggesting that

high flux magmatism during this time may have been initially fueled by a different process, due to a different tectonic setting (Monger et al., 1982; Crawford et al., 1987; Gehrels et al., 2008) than later 100 – 80 Ma magmatism.

Magmatic flux was quite low in the western CMB between 140-120 Ma (Gehrels et al., 2008), perhaps at least partially in response to an oblique sinistral component of plate convergence (Engebretson et al., 1985). Prior to the mid Cretaceous accretion of the allochthonous Alexander terrane, high magmatic flux was initiated during 120 – 100 Ma during which the Gravina Basin separated this terrane from North America and was accumulating of distal marine strata which suggests that early stages of this high-flux magmatism occurred in a regime of overall extension or sinistral transtension (Kapp and Gehrels, 1998; Gehrels et al., 2008). Based on this first order constraint, high flux magmatism from 120 – 100 Ma was not related to terrane accretion or crustal thickening, but perhaps due to the regional extension indicates a process such as decompression melting associated with mantle upwelling and back-arc spreading. Higher order geologic constraints from the location of magmatism during this time indicate that shut off of magmatism in eastern magmatic arc (Stikine Terrane) during prior to 110 Ma, was due to the southward movement of the outboard western arc active in Alexander-Wrangellia (Gehrels et al.,, 2008). Given these timing relations, the onset of high flux magmatism during 120 – 100 Ma may be related to the southward motion of Alexander-Wrangellia and the establishment of a single west facing magmatic arc (Crawford et al., 1987) that migrated eastward from the mid-Cretaceous until Eocene (Gehrels et al., 2008).

The timing of a magmatic flare-up event in the mid-late Jurassic (160 – 140 Ma) corresponds with a time of regional extension with evidence from the subsiding Bowser

Basin (MacIntyre et al., 2001) and Gravina Basin (Kapp and Gehrels, 1998) which is also hypothesized to be the outboard continuation of the Bowser Basin (Dickinson, 1976; van der Heyden, 1992). Constraints from calculations by Gehrels et al. (2008, Table 2), indicate that nearly 100% of the high flux magmatic event from 160 – 140 Ma occurred in the outboard Alexander-Wrangellia terrane. Data shown in Figures 5 and 6 indicates that Jurassic aged plutons which intrude Alexander-Wrangellia (open squares) show in part significantly more crustal Nd and Sr isotopic signatures compared to Stikine (closed triangles), which is unusual given the primitive nature of these terranes (Samson et al., 1989; Samson et al., 1990). A geologic control on source rock bulk and isotopic composition may explain these differences since the Late Jurassic to Early Cretaceous crustally evolved plutons (open squares Figures 5 and 6) intrude the a sequence of quartzite and marble, believed to be part of the Alexander terrane, but with considerably cratonic Nd and Sr isotopic signatures (Boghossian et al., 2000; Gehrels and Boghossian, 2000).

If these rocks, referred to as the Banks Island assemblage (Boghossian et al., 2000; Gehrels and Boghossian, 2000), are representative of a portion of the Alexander terrane which has a significantly more crustally evolved isotopic signature at depth, then the incorporation may explain the unusually crustally evolved signatures for some of the ~150 Ma aged plutons (Figures 5 and 6) emplaced into essentially an island arc setting where these signatures would not be expected. Another notable difference is that during the late Jurassic episode of high magmatic flux, $(La/Yb)_N$ reaches values of 20 – 40 in Alexander-Wrangellia intrusives (open squares, Figure 4). In comparison $(La/Yb)_N$ values of granitoid samples from the Stikine terrane which had little contribution the

magmatic flux (Gehrels et al., 2008) are ≤ 10 throughout the Jurassic which provides a geologic and geochemical constraint that garnet-rich igneous residues are formed only beneath centers of high magmatic flux.

During the late stages of the Eocene flare-up, the CMB was dominated by extensional tectonics and orogenic collapse in an arc increasingly dominated by normal faults (Andronicos et al., 2003; Hollister and Andronicos, 2006). In this study, maximum $(La/Yb)_N$ at 53 Ma (Figure 6) suggests that crustal thickening and deepening levels of magmagenesis continued until this time as the overthickened crust was collapsing under its own gravitational potential energy. The subduction of young and buoyant oceanic lithosphere of the Resurrection plate (Haeussler et al., 2003) may have promoted crustal thickening and high magmatic flux despite increasingly oblique plate convergence, while the collapse of the arc and cessation of CMB magmatism at 50-48 Ma may have resulted from complete removal of the Resurrection plate (Haeussler et al., 2003).

Poorly constrained relationships between the timing of movement along the eastern boundary detachment (Shames River detachment system) which was active between ~54 – 48 Ma (Andronicos et al., 2003; Rusmore et al., 2005) complicate models which invoke crustal extension to fuel high flux magmatism from 58 – 50 Ma. Since high flux magmatism, which initiated at ~60 Ma, pre-dates the onset of motion along the Shames River detachment system it is difficult to asses if the increased magmatism is the result of extension or vice versa. The gravitational collapse of the thermally weakened (as the result of high magmatic flux) and overthickened crust is the preferred interpretation based in the REE abundances determinined in this study which indicate deepening levels of magmagenesis from 70 – 53 Ma (Figure 4).

Crustal shortening and thickening until 53 Ma are consistent with the maximum $(La/Yb)_N$ at this time, after which crustal thinning proceeded as $(La/Yb)_N$ values decrease as the arc collapsed and magmatic flux dropped to less than half its peak by 50 Ma as the Resurrection plate neared complete removal. This is supported by the observation that data at 50 Ma have decreased $(La/Yb)_N$ of ~10 – 20 compared to $(La/Yb)_N$ = 30 - 60 during the peak of magmatism at ~53 Ma (Figures 4, 5 and 6). Further supporting the hypothesis that is that data from along the Douglas Channel (open triangles, Figures 5 and 6) indicate a steady isotopic evolution from 70 – 50 Ma which is more consistent with crustal shortening rather than extension (Barton, 1996). The significantly more crustal isotopic signatures observed in the Mathieson (open circles, Figures 5 and 6)and Burke/Dean transects (open squares, Figures 5 and 6) may be the result of a geologic control, that their isotopic signatures are influenced more by the somewhat crustally evolved Yukon-Tanana terrane (Samson et al., 1989)

Overall this data argues that the conditions surrounding the final Eocene high magmatic flux event were very similar to the previous event during the Mid Cretaceous which was fueled by crustal thickening. Although orogenic collapse certainly occurred in during the final stages of CMB magmatism, based on $(La/Yb)_N$ of this study significant thinning did not occur until after 53 Ma at which point the magmatic flux abruptly drops to less than half its 53 Ma peak (Figure 4) before shutting off completely by 48 Ma. Clearly the role of extensional or neutral stress states in the upperplate play some role in governing the magmatic flux, which may be very different during periods prior to terrane accretion (>100 Ma). It is apparent from this study that following the establishment of a single west facing arc in the mid Cretaceous (Crawford et al., 1987), the main mechanism

driving high magmatic flux, crustally evolved isotopic signatures, and increasing $(La/Yb)_N$ during 100 – 53 Ma was shortening in the upperplate.

Tectonic Models

Not fully addressed by crustal shortening and thickening alone, is the observation that Nd and Sr isotopic values abruptly change to primitive values accompanied by dramatically deceasing La/Yb_N during low magmatic flux from 140 – 120 Ma and 80 – 60 Ma, but specifically for 80 – 70 Ma for which there is strong geologic constraints to investigate these changes (Figures 4, 5, and 6). A viable tectonic model explaining the isotopic and geochemical trends observed in the CMB during a change from high to low flux magmatism must satisfy: 1) the cyclically changing proportions of mantle to crustal contributions in the source of these magmas, which is manifested in the changes between primitive and evolved Nd and Sr isotopic signatures; 2) the cyclic variation in $(La/Yb)_N$, or changes in crustal thickness and garnet stability as a residual phase; 3) explain why changes in Nd and Sr isotopic signatures and $(La/Yb)_N$ are correlated with magmatic flux; 4) account for deformation in the upperplate associated with known terrane accretionary and translation events in the Canadian Cordillera; and 5) must occur over timescales of 10 – 20 My, as indicated by the data shown in Figures 4, 5, and 6.

Viable tectonic models shown in Figure 8, include Model 1 in which the isotopic and geochemical trends and magmatic flux are driven purely by deformation in the upperplate, and Models 2 and 3 where the trends are driven by deformation in the

upperplate (Model 1) plus gravitational instabilities beneath the upperplate. These mechanisms are Rayleigh-Taylor instabilities and a mantle lithospheric delamination event, respectively for Model 2 and Model 3. In Model 1, the initially primitive isotopic signatures observed during low flux magmatism can be explained as being dominated by a mantle source until crustal shortening and underthrusting result in the perturbation of geotherms to temperatures exceeding the wet solidi of appropriate lower crustal lithologies. Upon reaching the wet solidus of an assemblage of lower crustal rocks, dehydration melting of micas and amphiboles occurs (Guo-Neng and Grapes, 2007) and may fuel a magmatic flare-up.

Model 1 would thus provide a mechanism, underthrusting, to fuel high flux magmatism and its corollary with more "crustal" Nd and Sr isotopic signatures and elevated $(La/Yb)_N$ (increased garnet stability) of these rocks due to increased crustal melting and thickening crust. One shortcoming of this model however, is that crustal thickening alone can not account for the changes to primitive isotopic signatures (increased mantle input to source) and decreased $(La/Yb)_N$ (garnet poor residual assemblage) observed during periods of low magmatic flux. These factors all indicate shallower, not deeper, levels of magma genesis. An increase in mantle magma contributions would be contradictory to what is known about magmatism related to a thickening column of radiogenic heat producing elements and thermal relaxation associated with thick crust (England and Thompson, 1984, 1986; Karabinos and Ketcham, 1988; Zen, 1988; Patino-Douce et al, 1990). Model 2 or Model 3 are viable alternatives, and can account for the deficiencies in Model 1 since they account for

dynamic processes occurring beneath the upperplate that may not be solely related to rates of plate convergence and deformation.

Model 2 and Model 3 consider the consequence of partially melting the lower crust, which is that dry granulite faces metamorphic lower crustal rocks are created. The implication of creating granulites is that to maintain the high magmatic flux, fertile (mica and amphibole rich) lithologies must continue to be underthrust into the lower crust. In Models 2 and 3 the continued shortening and thickening in the upperplate which fuel high flux magmatism eventually induce a negative feedback, and are responsible for stifling the magmatic flux when hydrous lithologies are no longer available. The space problem associated with extreme lithospheric shortening resulting in the crowding of the wedge beneath the arc with mantle lithosphere (DeCelles, 2004) is proposed as a mechanism to inhibit the availability, due to decreased rate of underthrusting and inhibited melting, of melt-fertile lithologies in the CMB during 140 – 120 Ma and 80 – 60 Ma.

Low flux magmatism will persist until the space problem that results from lithospheric crowding and inhibited melting is alleviated and rapid underthrusting resumes. If sufficiently thick, the basaltic component of mantle lithosphere crowding the wedge may undergo phase changes to denser eclogite facies, causing the lithosphere to be recycled as "cold-blobs" (Anderson, 2006). This phase transformation may promote the development of a Rayleigh-Taylor instability (Model 2) or a peel back delamination, as similarly proposed by Bird (1979), which may remove lithosphere up to the base of (and possibly including) the lower crust (Model 3) (Figure 8). The process of lithospheric thinning is inferred to explain the dramatic change to decreased $(La/Yb)_N$ due to decreased levels of magma genesis and decreased garnet stability. The change to

primitive isotopic signatures observed during 80 – 70 Ma, and sustained during 140 – 120 Ma and 80 – 60 Ma (Figures 4, 5, and 6) may be explained by the dominance of a basaltic decompression melts due to the replacing of foundering or delaminating lithosphere with upwelling asthenosphere. In Figure 8, the thin black arrows indicate a return flow of asthenospheric mantle replacing the descending mantle instability. A low amount of crustal melts and isotopically primitive signatures will persist until rapid underthrusting and melting of lower crustal lithologies resumes once the space problem beneath the arc has been alleviated.

Periods of low magmatic flux in this sense are significant to the evolution of the CMB since this is a time of priming the arc for another flare-up as the orogenic cycle continues. Thinning the lithosphere by delamination alleviates the space problem in the crowded mantle wedge beneath the arc and allows for a positive feedback in the arc as rapid underthrusting may resume. Renewed crustal shortening and underthrusting can proceed at high rates once the space problem beneath the arc is resolved (DeCelles, 2004) and creates the conditions necessary for the next flare-up: thick and hot fertile (mica and amphibole rich) crust pushed to deep levels where it can partially melt and assimilate with melts of underplated basaltic crust or primary mantle. Models 2 and 3 are also able address issues associated with the development of dense garnet-rich (up to ~50%) residues which may be negatively buoyant and prone to detaching from the crust and sinking into the mantle (Kay and Kay, 1991; Ducea and Saleeby, 1996; Ducea, 2001).

The ability of a lower crustal or residual igneous residuum to initiate a gravitational instability such as proposed in Model 2 is dependent upon its density and viscosity compared to underlying mantle lithosphere (Jull and Kelemen, 2001). Thus in

Model 2, a Raleigh-Taylor instability may be driven by the foundering of an eclogitic root (Ducea, 2002) or foundering cold mantle lithosphere (DeCelles, 2004), or both mechanisms may be acting at the same time. Rather than being driven by density and viscosity alone, Model 3 requires a mechanical process to break through the mantle lithosphere and enable asthenosphere to contact the crust so that the "peeling" may proceed (Bird, 1979). This process is illustrated in Figure 8, and is hypothesized to initiate as thick dense eclogitized lithospheric mantle becomes pulled down by the descending oceanic plate. The resulting gap formed allows for asthenospheric mantle to replace the delaminating lithospheric mantle and drive isotopic signatures to more primitive values, and possibly also an outlet for dense garnet-rich igneous residues.

Both Model 2 and Model 3 are able to explain fluctuations in mantle to crustal contributions to magmas, garnet stability as a residual phase, and magmatic flux for the CMB. It may be possible to distinguish between these tectonic models in the CMB by considering their effects on heat flow and magmagenesis. It is noteworthy that the localized mantle upwelling to the base of the crust which would be invoked by Model 3 may help to explain the orogen parallel localized zone of steep tabular tonalitic plutons also known as the Great Tonalite Sill (GTS) (Brew and Ford, 1978; Ingram and Hutton, 1994). Ingram and Hutton (1994) proposed the gravitational removal of lithospheric mantle beneath overthickened continental crust as a mechanism for a focused zone of upwelling asthenosphere; although this may be a viable hypothesis, the delamination proposed in Model 3 also provides a mechanism to generate the GTS and fits into a broader tectonic context. Coast Shear zone intrusives which are ~60 Ma (Tables 1 and 2) may support this hypothesis, as their primitive isotopic signatures and low $(La/Yb)_N$

suggest that their genesis occurred following a lithospheric thinning event. The potential removal of garnet-rich batholithic roots following the final Eocene magmatic flare-up may be more likely to occur via a Rayliegh-Taylor gravitational instability (Model 2) rather than a delamination since the end of subduction ~50 Ma makes it difficult to initiate the "peeling" illustrated in Model 3 (Figure 8).

Based on Model 1 which is viable to explain the tectonic processes leading to a magmatic flare-up, and Models 2 and 3 which also can account for the tectonic processes leading to a magmatic lull, an orogenic cycle may be defined in the CMB which took place from 100 – 70 Ma. This cycle consist of two stages: "root-forming" and "root-removing." The root-forming stage (Model 1) is related to shortening and thickening of crust and mantle lithosphere, and the formation of dense igneous residues which are believed to be at least 1:1 volume proportion to the plutonic rocks (Ducea, 2001). The root-removing stage is characterized by gravitational foundering (Model 2) or mechanical peeling (Model 3) of overthickened crust, mantle lithosphere, and/or igneous residues.

The cycle repeats as the formation and removal of batholithic roots induce both positive and negative feedback to the arc magmatic flux by controlling rate of deformation in the upperplate, and proportion of crustal to mantle magma sources. Geologic constraints and the Nd and Sr isotopic, and REE abundances of CMB plutonic rocks (Figures 4, 5, and 6), suggest that igneous root formation and removal occurred Mid – Late Cretaceous primarily in response to crustal shortening. Similar isotopic and geochemical trends also support crustal shortening as the driving mechanism for the final Eocene high magmatic flux event, despite these similarities the mechanisms of the Mid – Late Jurassic high flux magmatism remain uncertain. It is clear that based on $(La/Yb)_N$

(Figure 4) that garnet-rich igneous residues were formed in each period of high magmatic flux, and that there is strong evidence supporting the removal of these garnet-rich batholithic roots during periods of low magmatic flux.

Conclusions

The CMB provides an excellent natural laboratory to examine the mechanisms which operate during the evolution of a magmatic arc. This study has shown that for the CMB that there is a clear correlation between fluctuations in magmatic flux and the observed episodicity in Nd and Sr isotopic signatures and REE abundances, enabling the unique ability to probe the mechanisms of magmatism and magmatic evolution in this arc. Important findings from our study are as follows:

● 80 plutonic rock samples were analyzed for their Nd and Sr isotopic characteristics, which confirmed the juvenile nature of the southern CMB.

● The systematic variation through time, and with magmatic flux, of REE abundances in all of the rocks in this study, indicate a cyclic fluctuation in lithospheric thickness, depth of magmagenesis, and evidence for the formation and removal of dense garnet-rich igneous residues.

● Variations among Nd and Sr isotopic systems are also well correlated through time, with REE variations and magmatic flux, indicating cyclically changing proportions of mantle to crustal magma sources.

● For the geologically well constrained periods 100 – 80 Ma, and 70 – 53 Ma high flux magmatism, crustally evolving isotopic signatures, and the formation of garnet-rich

igneous residues were fueled by crustal thickening related to terrane accretionary and translation events

● For the geologically well constrained period 80 - 70 Ma low flux magmatism, primitive isotopic signatures, and the formation of garnet-poor igneous residues are interpreted to have resulted from the removal, via delamination or foundering, of dense garnet-rich batholithic roots formed during the previous high magmatic flux event.

●A comparison of the isotopic and geochemical trends observed during 200 – 50 Ma, and those from the geologically well constrained period of 100 – 70 Ma, suggest that the formation and removal of batholithic roots was an on going and cyclic process in the CMB.

●There is strong evidence to show that in the CMB garnet-rich batholithic roots were likely removed following their formation in high flux magmatic events that took place in the Mid -Late Jurassic, Mid – Late Cretaceous, and Eocene.

●The final Eocene root removal event is not documented in the isotopic characteristics of plutonic rocks because the cessation of magmatism in the CMB precludes the completion of the final orogenic cycle while the arc was still active.

REFERENCES

Anders, E., and Grevesse, N. (1989). Abundances of the elements: Meteoric and Solar. Gechimica et Cosmo Chimica Acta 53: 197 - 214.

Anderson, D. L. (2006). The eclogite engine: Chemical geodynamics as a Galileo thermometer, in The Origins of Melting Anomalies: Plates, Plumes, and Planetary Processes, A GSA Book (in preparation), Editors: Gillian R. Foulger & Donna M. Jurdy.

Andronicos, C. L., Chardon, D., Gehrels, G., Hollister, L.S., and Woodsworth, G.J., (2003). Strain partioning in an obliquely convergent orogen, plutonism, and synorogenic collapse: Coast Mountain Batholith, British Columbia, Canada. Tectonics 22(no. 2): 1012, doi:10.1029/2001TC0010312.

Andronicos, C.L., Hollister, L.S., Davidson, C., and Chardon, D., (1999). Kinematics and tectonic significance of transpressive structures within the Coast plutonic complex, British Columbia. J. Struct. Geol. 21: 229 - 243.

Armstrong, R. L. (1988). Mesozoic and early Cenozoic evolution of the Canadian Cordillera. In Processes in continental lithospheric deformation. Edited by S.P. Clark, B.C. Burchfield, and J. Suppe. . Geological Society of America, Special Paper 218: 55 - 91.

Barker, F., and Arth, J.G. (1984). Preliminary results, Central Gneiss Complex of the Coast Range Batholith, southeastern Alaska: the roots of a high-K, calc alkaline arc? Physics of the Earth and Planetary Interiors 35: 191 - 198.

Barton, M.D. (1996). Granitic magmatism and metallogeny of southwestern North America: Transactions of the Royal Society of Edinburgh, Earth Sciences, v. 87, 261-280.

Bird, P. (1979). Continental delamination and the Colorado Plateau. J. Geophys. Res. 84: 7561 - 7571.

Brew, D. A., and Ford, A.B. (1978). Megalineament in southeastern Alaska marks southwest edge of Coast Range batholithic complex. Can. J. Earth Sci. 15: 1763 - 1772.

Brew, D. A., Himmelberg, G.R., Loney, R.A., and Ford, A.B. (1992). Distribution and characterization of metamorphic belts in the southern Alaska part of the North American Cordillera. Journal of Metamorphic Geology 10: 465 - 482.

Coney, P. J., Jones, D.L., and Monger, J.W.H. (1980). Cordilleran Suspect Terranes. Nature 288: 329-333.

Coney, P. J., and Jones, D.L. (1985). Accretion tectonics and crustal structure in Alaska. Tectonophysics 119: 265-283.

Crawford, M. L., and Hollister, L.S. (1982). Contrast of metamorphic and structural histories across the Work Channel Lineament, Coast Plutonic Complex, British Columbia. Journal of Geophysical Research 87(no. B5): 3849 - 3860.

Crawford, M. L., Hollister, L.S., and Woodsworth, G.J. (1987). Crustal deformation and regional metamorphism across a terrane boundary, Coast Plutonic Complex, British Columbia. Tectonics 6(no. 3): 343 - 361.

Crawford, M. L., Gehrels, G.E., Klepeis, K.A., and Crawford, W.A. (1997). Latest Cretaceous and Paleogene history of the central region of the Coast orogen at the British Columbia - Alaska border: Geological Society of America Abstracts with Programs 29, no.6: p.83.

Cui, Y., and Russell, J.K. (1995). Nd - Sr - Pb isotopic studies of southern Coast Plutonic Complex, southwestern British Columbia. GSA Bulletin 107(no. 2): 127 - 138.

DeBari, S. M. (1997). Evolution of magmas in continental and oceanic crust: The role of the lower crust. Canadian Mineralogist 35: 505 - 515.

DeCelles, P. G. (2004). Late Jurassic to Eocene evolution of the cordilleran thrust belt and foreland basin system, Western U.S.A. American Journal of Science 304: 105 - 168.

DePaolo, D. J. (1981). Trace element and isotopic effects of combined wallrock assimilation and fractional crystalization. Earth and Planetary Science Letters 53: 189 - 202.

Dickinson, W.R. (1976). Sedimentary basins developed during evolution of Mesozoic–Cenozoic arc-trench systems in western North America. Can. J Earth Sci. 13: 1268 - 1287

Driver, L. A., Creaser, R.A., Chacko, T., and Erdmer, P. (2000). Petrogenesis of the Cretaceous Cassiar batholith, Yukon-British Columbia, Canada: Implications for magmatism in the North American Cordilleran Interior. GSA Bulletin 112(no. 7): 1119 - 1133.

Ducea, M. N., and Saleeby, J.B. (1996). Buoyancy sources for a large, unrooted mountain range, the Sierra Nevada, California: Evidence from xenolith thermobarometry. Journal of Geophysical Research 101(no. B4): 8229 - 8244.

Ducea, M. N., and Saleeby, J.B. (1998). The age and origin of a thick-ultramafic keel from beneath the Sierra Nevada batholith. Contrib Mineral Petrol 133: 169 - 185.

Ducea, M. N. (2001). The California arc: Thick granitic batholiths, eclogitic residues, lithospheric scale thrusting, and magmatic flare-ups. Geological Society of America: GSA Today 11: 4 - 10.

Ducea, M. N. (2002). Constraints on the bulk composition and root foundering rates of continental arcs: A California arc perspective. Journal of Geophysical Research 107(no. B11): 2304, doi:10.1029/2001JB000643.

Ducea, M. N., and Barton, M.D. (2007). Igniting flare-up events in Cordilleran arcs. Geology 35(no. 11): 1047 - 1050.

Dufek, J., and Bergantz, G.W. (2005). Lower Crustal Magma Genesis and Preservation: a Stochastic Framework for the Evaluation of Basalt - Crust Interaction. Journal of Petrology 46(11): 2167 - 2195 doi:10.1093/petrology/egi049.

Engebretson, D. C., Cox, A., and Gordon, R.G. (1985). Relative motions between oceanic and continental plates in the Pacific Basin: Geological Society of America Special Paper 206. 59p.

England, P. C., and Thompson, A.B. (1986). Processes of Collision Orogeny. Geological Society, London, Special Publications, 1986 19: 83 - 94.

Friedman, R. M., Mahoney, J.B., and Cui, Y. (1995). Magmatic evolution of the southern Coast Belt: constraints from Nd-Sr isotopic systematics and geochronology of the southern Coast Plutonic Complex Can. J. Earth Sci. 32: 1681-1698.

Frost, B. R., Barnes, C.G., Collins, W.J., Arculus, R.J, Ellis, D.J., and Frost, C.D. (2001). A geochemical classification for granitic rocks. Journal of Petrology 42(11): 2033 - 2048.

Gehrels, G. E., McClelland, W.C., Samson, S.D., Patchett, P.J., and Jackson, J.L. (1990). Ancient continental margin assemblage in the norther Coast Mountains, southeast Alaska and northwest Canada. Geology 18: 208 - 211.

Gehrels, G. E. (2001). Geology of the Chatham Sound region, southeast Alaska and Coastal British Columbia. Can. J. Earth Sci. 38: 1579 - 1599.

Gerbi, C., Johnson, S.E., and Koons, P.O. (2006). Controls on low-pressure anatexis. Journal of Metamorphic Geology 24: 107 - 118.

Ghent, E. D., Dipple, G.M., and Russell, J.K. (2004). Thermodynamic models for eclogitic mantle lithosphere. Earth and Planetary Science Letters 218: 451 - 462.

Ghosh D.K. and Lambert, R. S. J. (1995). Nd - Sr isotope geochemistry and petrogenesis of Jurassic granitoid intrusives, southeast British Columbia, Canada in Miller, D.M., and Busby, C., Jurassic Magmatism and Tectonics of the North American Cordillera: Boulder, Colorado, Geological Society of America Special Paper 299

Ghosh, D. K. (1995). Nd - Sr isotopic constrains on the interactions of the Intermontane Superterrane with the western edge of North America in the southern Canadian Cordillera. Can. J. Earth Sci. 32: 1740 - 1758.

Guo-Neng, C., and Grapes, R. (2007). Granite Genesis: In-Situ Melting and Crustal Evolution. Netherlands, Springer.

Haeussler, P., Bradley, D., Wells, R., Miller, M., 2003, Life and death of the Resurrection plate: Evidence for its existence and subduction in the northeastern Pacific in Paleocene-Eocene time: Geological Society of America Bulletin, v. 15, no. 7, p. 867-880.

Hollister, L. S. (1982). Metamorphic evidence for rapid (2mm/yr) uplift of a portion of the central gneiss complex, Coast Mountains, B.C. Canadian Mineralogist 20: 319 - 322.

Hollister, L. S., and Andronicos, C.L. (2000). The Central Gneiss Complex, Coast Orogen, British Columbia. Special Paper Geological Society of America 343: 45 - 59.

Hollister, L. S., and Andronicos, C.L. (2006). Formation of new crust in Western British Columbia during transpression and transtension. Earth and Planetary Science Letters 249: 29 - 38.

Ingram, G. M., and Hutton, D.H.W. (1994). The Great Tonalite Sill; emplacement into a contractional shear zone and implications for Late Cretaceous to Early Eocene tectonics in Southeastern Alaska and British Columbia. Geological Society of America Bulletin 106: 715 - 728.

Jones. D.L, S., N.J., and Hillhouse, J. (1977). Wrangellia -a displaced terrane in northwestern North America. Can. J. Earth Sci. 14: 2565-2577.

Jull, M., and Kelemen, P.B. (2001). On the conditions for lower crustal instability. Journal of Geophysical Research 106(no B6): 6423 - 6446.

Kapp, P.A., and Gehrels, G.E. (1998). Detrital zircon constraints on the tectonic evolution of the Gravina belt, southeastern Alaska. Can J. Earth Sci. 35: 253 - 268

Karabinos, P., and Ketcham, R. (1988). Thermal structure of active thrust belts. J. Metamorphic Geol. 6: 559 - 570.

Kay, S. M., Godoy, E., and Kurtz, A. (2005). Episodic arc migration, crustal thickening, subduction erosion, and magmatism in the south-central Andes. Geological Society of America Bulletin 117(1/2): 67 - 88.

Klepeis, K. A., Crawford, M.L., and Gehrels, G.E. (1998). Structural history of the crustal-scale Coast shear zone north of Portland Canal, southeast Alaska and British Columbia. Jounal of Structural Geology 20(7): 883 - 904.

Lonsdale, P. (1988). Paleogene history of the Kula plate: Offshore evidence and onshore implications. Geological Society of America Bulletin 100: 733 - 754.

MacIntyre, D. G., Villeneuve, M.E., and Schiarizza, P. (2001). Timing and tectonic setting of Stikine Terrane magmatism, Babine-Talka area, central British Columbia. Can. J. Earth Sci. 38: 579 - 601.

Mc Clelland, W. C., Gehrels, G.E., Samson, S.D., and Patchett, P.J. (1992). Structural and geochronologic relations along the western flank of the Coast Mountains Batholith: Stikine River to Cape Fanshaw, central southeastern Alaska. Jounal of Structural Geology 14: 475 - 489.

Monger, J. W. H., Price, R.A., and Tempelman-Kluit, D.J. (1982). Tectonic accretion and the origin of the two major metamorphic and plutonic welts in the Canadian Cordillera. Geology 10: 70 - 75.

Monger, J. W. H., van der Heyden, P., Journeay, J.M., Evenchick, C.A., and Mahoney, J.B. (1994). Jurassic-Cretaceous basins along the Canadian Coast Belt: Their bearing on pre-mid-Cretaceous sinistral displacements. Geology 22: 175 - 178.

Monger, J. W. H. (2002). Canadian Cordillera: Geology and Tectonic Evolution. CSEG Recorder: 17 - 36.

Patchett, P. J., and Ruiz, J. (1987). Nd isotopic ages of crust formation and metamorphism in the Precambrian of eastern and southern Mexico. Contrib Mineral Petrol 96: 523-528.

Patchett, P. J., Gehrels, G.E, and Isachsen, C.E. (1998). Nd isotopic characteristics of metamorphic and plutonic rocks of the Coast Mountains near Prince Rupert, British Columbia. Can. J. Earth Sci. 35: 556-561.

Patino Douce, A. E., Humphreys, E.D., and Johnston, A.D. (1990). Anatexis and metamorphism in tectonically thickened continental crust exemplified by the Sevier hinterland, western North America. Earth and Planetary Science Letters 97: 290 - 315.

Rapp, R. P., and Watson, B.E. (1995). Dehydration Melting of Metabasalt at 8-32 kbar: Implications for Continental Growth and Crust-Mantle Recycling. Journal of Petrology 36(4): 891 - 931.

Roddick, J. A., and Hutchinson, W.W. (1974). Setting of the Coast Plutonic Complex, south of latitude 55^0N. . Pacific Geology 8(91 - 108).

Rubin, C. M., Saleeby, J.B., Cowan, D.S., Brandon, M.T., and McGroder, M.F. (1990). Regionally extensive mid-Cretaceous west-vergent thrust system in the northwestern Cordillera: Implications for continental margin tectonism. Geology 18: 276-280.

Rushmer, T. (1993). Experimental high pressure granulites: some applications to natural mafic xenolith suites and Archean granulite terranes. Geology 21(5): 411 - 414.

Rusmore, M. E., and Woodsworth, G.J. (1991). Distribution and tectonic significance of Upper Triassic terranes in the eastern Coast Mountains and adjacent Intermontane Belt, British Columbia. Can. J. Earth Sci. 28: 532 - 541.

Rusmore, M. E., Woodsworth, G.J., and Gehrels, G.E. (2005). Two-stage exhumation of midcrustal rocks, Coast Mountains, British Columbia. Tectonics 24: 25 pp., doi:10.1029/2004TC001750.

Samson, S. D., McClelland, W.C., Patchett, P.J., and Gehrels, G.E. (1989). Evidence from neodymium isotopes for mantle contributions to Phanerozoic crustal genesis in the Canadian Cordillera. Nature 37: 705-709.

Samson, S. D., Patchett, P.J., Gehrels, G.E., and Anderson, R. (1990). Nd and Sr isotopic characterization of the Wrangellia terrane and implications for crustal growth of the Canadian Cordillera. Journal of Geology 98: 749 - 762.

Samson, S. D., and Patchett, P.J. (1991). The Canadian Cordillera as an analogue of Proterozoic crustal growth. Australian Journal of Earth Sciences 38: 595 - 611.

Samson, S. D., Patchett, P.J., McClelland, W.C., and Gehrels, G.E. (1991a). Nd isotopic characterization of metamorphic rocks in the Coast Mountains, Alaskan, and Canadian Cordillera: Ancient crust bounded by juvenile terranes. Tectonics 10(no. 4): 770 - 780.

Samson, S. D., Patchett, P.J., McClelland, W.C., and Gehrels, G.E. (1991b). Nd and Sr constraints on the petrogenesis of the west side of the northern Coast Mountains batholith, Alaskan and Canadian Cordillera. Can. J. Earth Sci. 28: 939 - 946.

Taylor, S.R., and McLennan, S.M. (1985). The continental crust: Its composition and evolution. Blackwell Scientific Pub., Palo Alto, CA.

Thompson, P. C., and England, A.B. (1984). Pressure - Temperature - Time Paths of Regional Metamorphism I. Heat Transfer during the Evolution of Regions of Thickened Continental Crust. Journal of Petrology 25(Part 4): 894 - 928.

Thorkelson, D. J., and Taylor, R.P. (1989). Cordilleran slab windows. Geology 17: 833 - 836.

Unterschutz, J. L. E., Creaser, R.A., Erdmer, P., Thompson, R.I., and Daughtry, K.L. (2002). North American margin origin of Quesnel terrane strata in the southern Canadian Cordillera: Inferences from geochemical and Nd Isotopic characteristics of Triassic metasedimentary rocks GSA Bulletin 114(no. 4): 462 - 475.

van der Heyden, P. (1992). A middle Jurassic to Early Tertiary Andean-Sierran arc model for the coast belt of British Columbia. Tectonics 11(no. 1): 82 - 97.

Weill, D. F., and Drake, M.J. (1973). Europium Anomaly in Plagioclase Feldspar: Experimental Results and Semiquantitative Model. Science, New Series 180(4090): 1059-1060.

Wheeler, J. O., and McFeely, P. (1991). Tectonic assemblage map of the Canadian Cordillera: Geological Survey of Canada Map 1712A.

Zen, E. (1988). Thermal modelling of stepwise anatexis in a thrust-thickened sialic crust. . Transactions of the Royal Society of Edinburgh: Earth Sciences 79: 223 - 235.

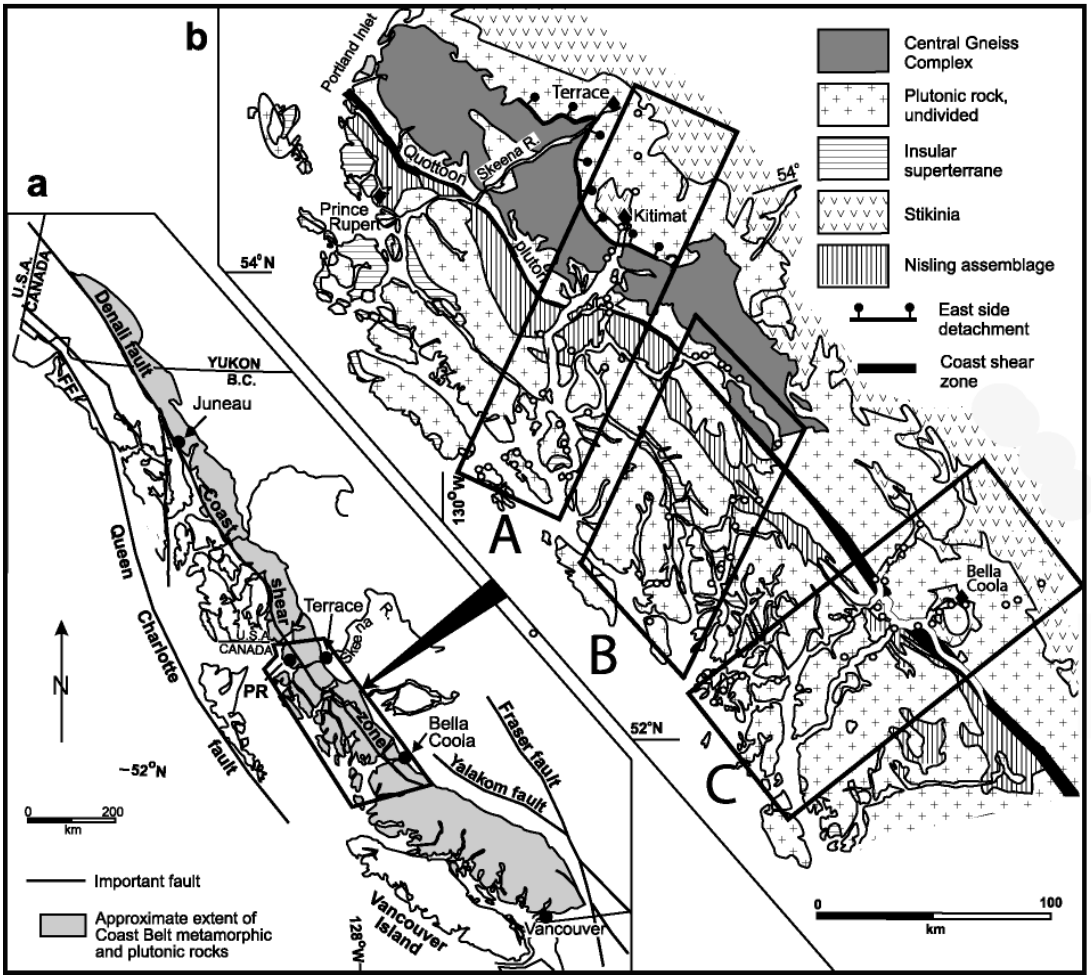

Figure 1: Location of BATHOLITHS study area. **(**a) Extent of Coast Belt plutonic and metamorphic rocks, and major Tertiary Faults. (b) Regional geologic map showing sample locations (open circles), which are located primarily along three transects across the arc located in the Douglas Channel (A), Mathieson Channel (B) and Burke/Dean Channels (C). Sample locations are shown as open circles. Modified from Rusmore et al. (2005).

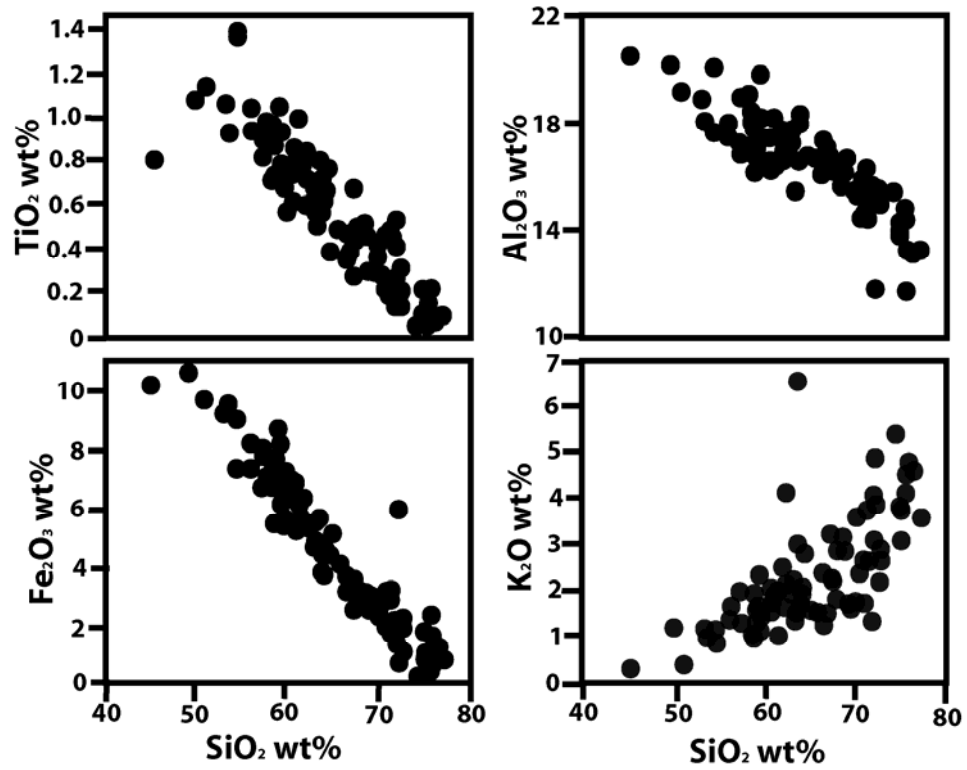

Figure 2: Harker diagrams for CMB plutonic rocks. Note variation among oxides with increasing silica; these trends are interpreted to result from the mixing between low silica (mantle) and high silica (crustal) magma sources.

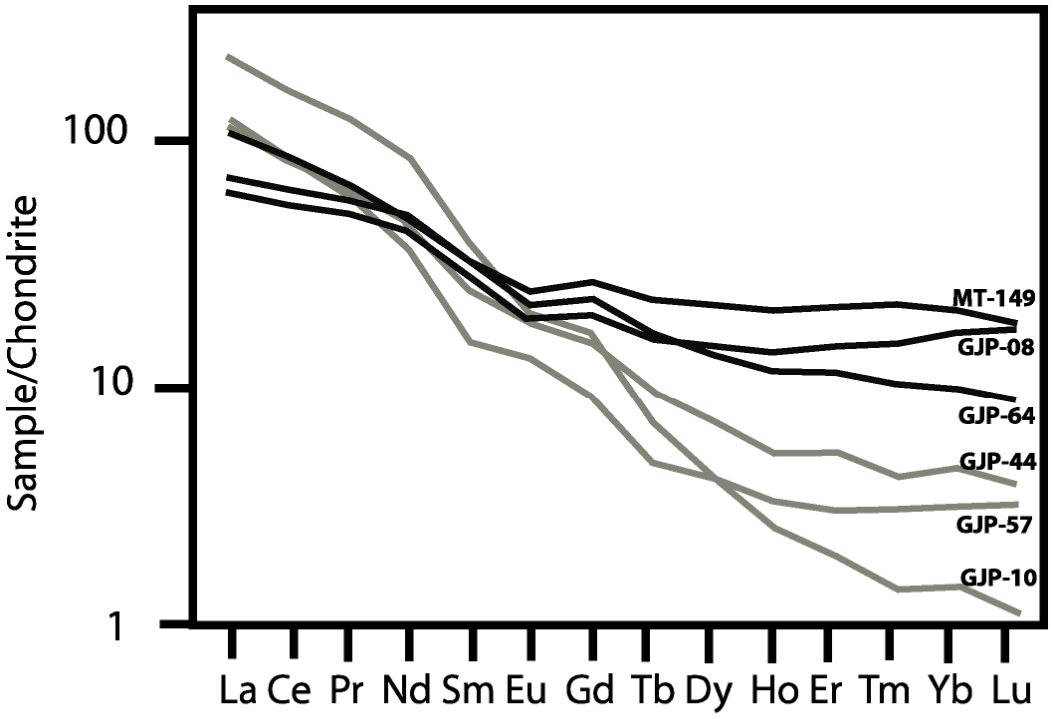

Figure 3: Chondrite-normalized REE distributions for selected CMB samples formed during high flux magmatism (grey) and low flux magmatism (black). Note the bimodal nature for these samples which display much "steeper" REE plots when generated during high flux magmatism.

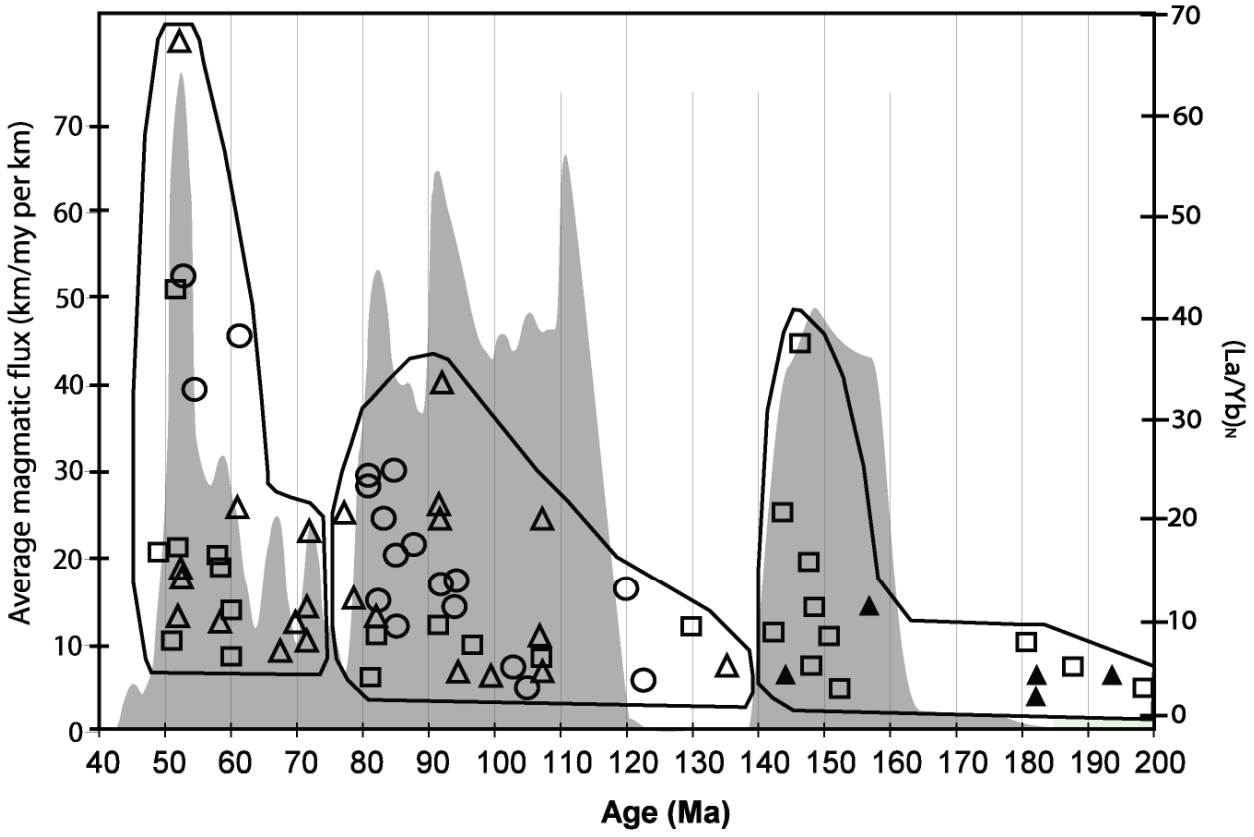

Figure 4: (La/Yb)n for CMB samples of this study. The left vertical axis is scaled for fluctuations in magmatic flux (grey). Open squares (Douglas Channel), open circles (Mathieson Channel), and open and closed triangles (Burke/Dean Channels) correspond with to the right vertical axis which is scaled for variations in $(La/Yb)_N$. For Jurassic aged samples the closed triangles represent samples from the Stikine Terrane, open triangles are from the Alexander-Wrangellia terrane, see text for discussion

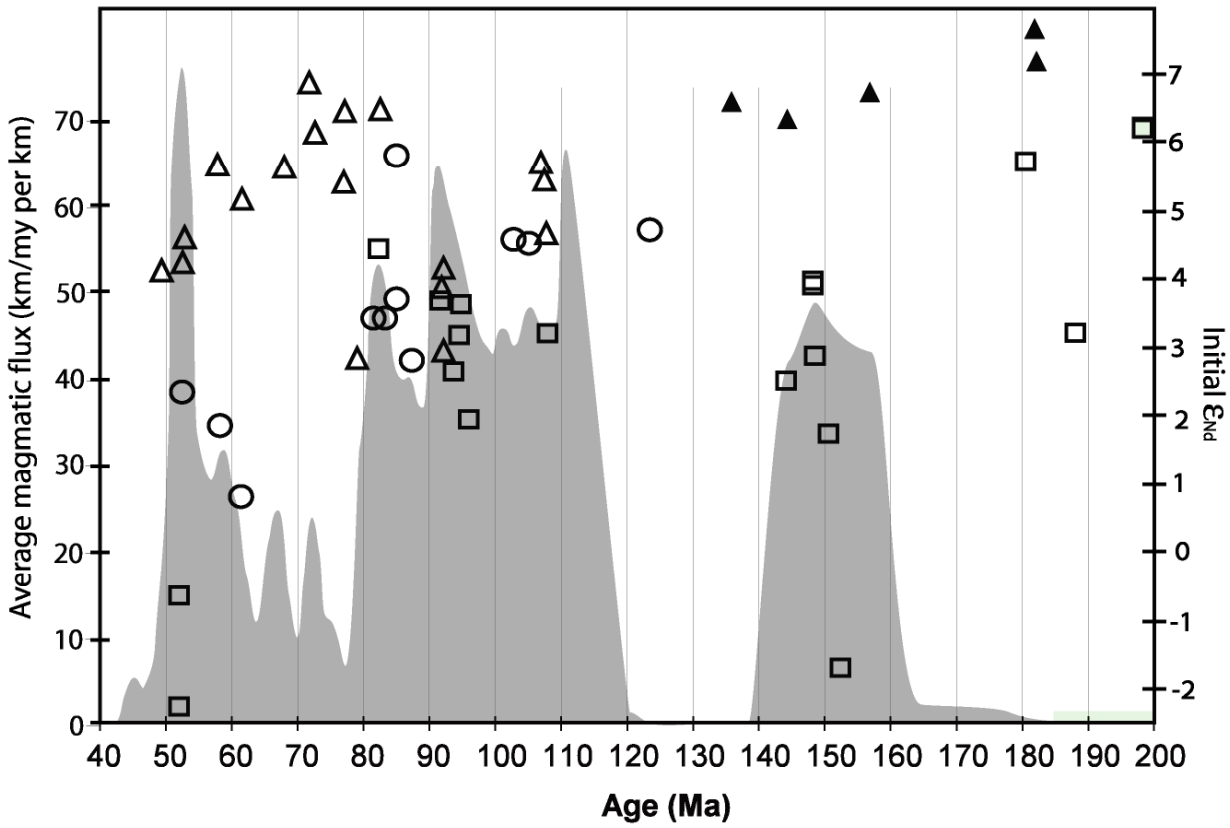

Figure 5: Initial εNd for CMB samples of this study. The left vertical axis is scaled for fluctuations in magmatic flux (grey). Open squares (Douglas Channel), open circles (Mathieson Channel), and open and closed triangles (Burke/Dean Channels) correspond with to the right vertical axis which is scaled for variations in ε_{Nd}. For Jurassic aged samples the closed triangles represent samples from the Stikine Terrane, open triangles are from the Alexander-Wrangellia terrane, see text for discussion

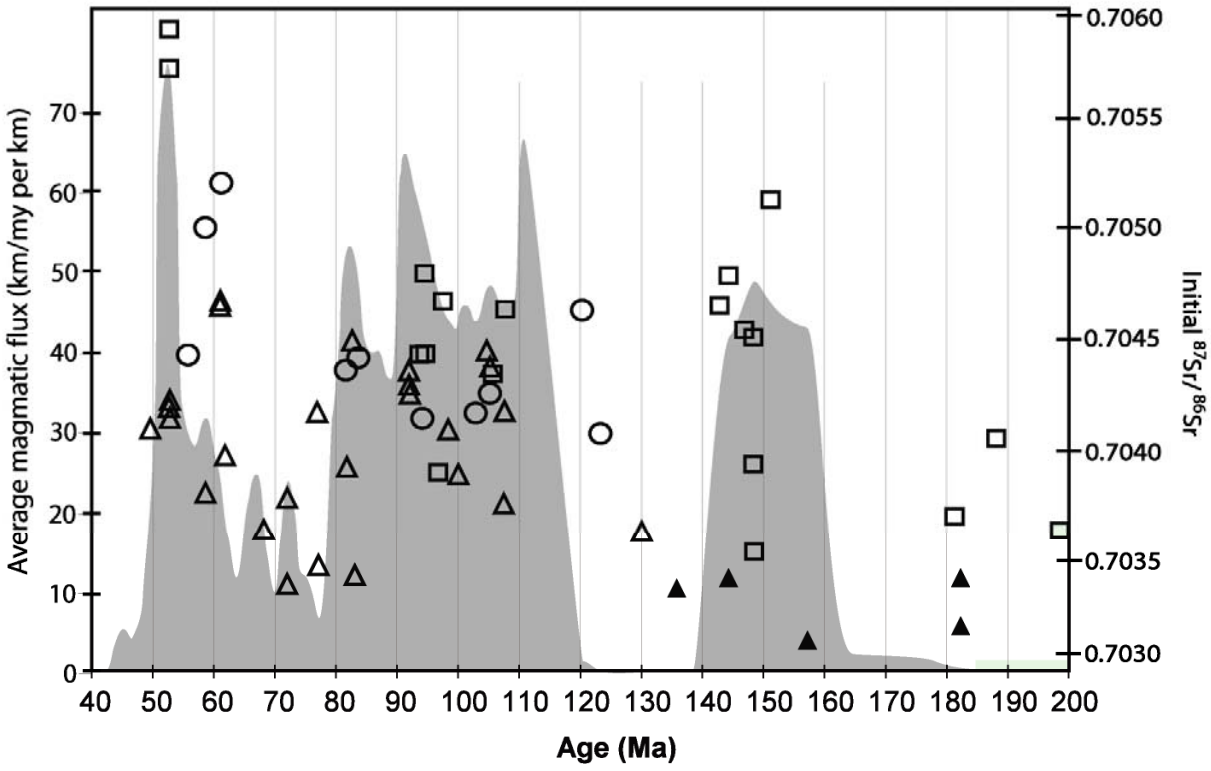

Figure 6: Initial $^{87}Sr/^{86}Sr$ for CMB samples of this study. The left vertical axis is scaled for fluctuations in magmatic flux (grey). Open squares (Douglas Channel), open circles (Mathieson Channel), and open and closed triangles (Burke/Dean Channels) correspond with to the right vertical axis which is scaled for variations in $^{87}Sr/^{86}$ Sr. For Jurassic aged samples the closed triangles represent samples from the Stikine Terrane, open triangles are from the Alexander-Wrangellia terrane, see text for discussion.

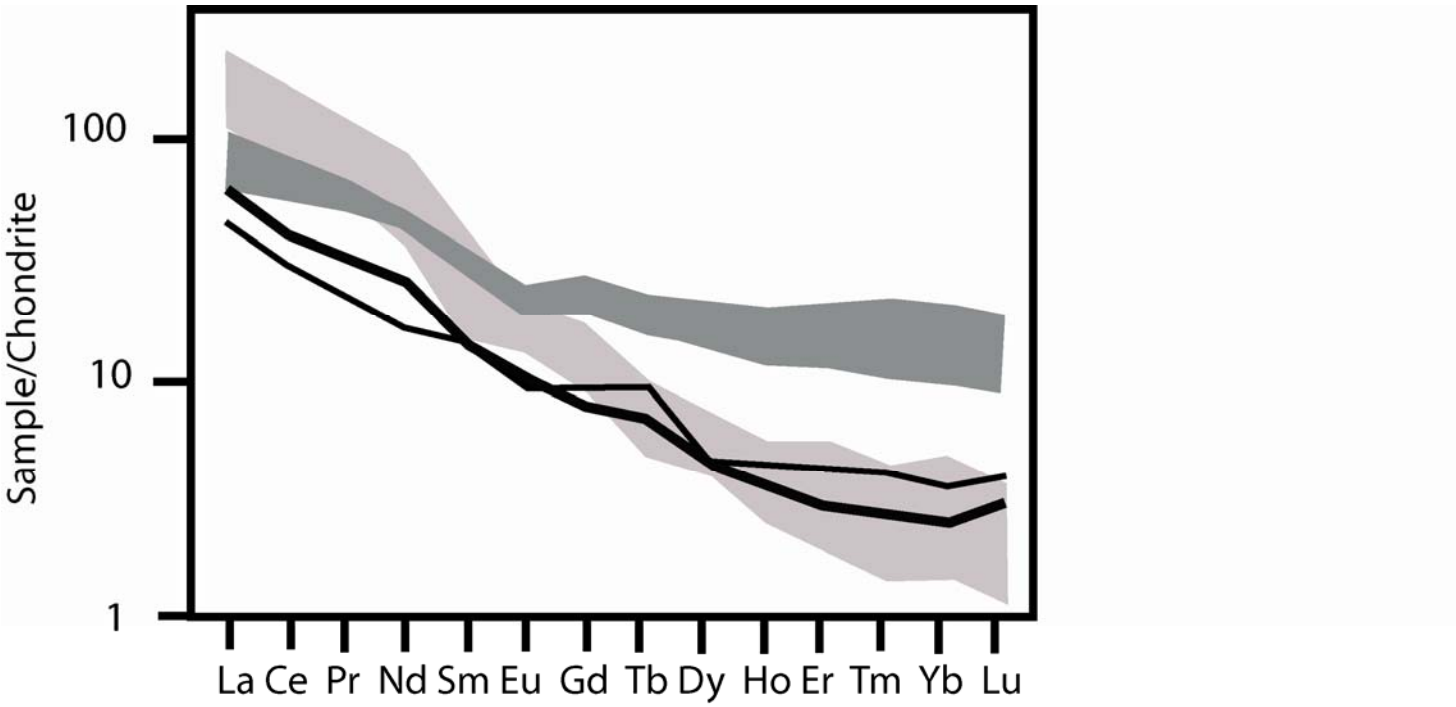

Figure 7: Chondrite-normalized REE distributions for the average Central Sierra Nevada Batholith (CSNB) tonalite (thin line) and granodiorite (thick line) samples (Dodge et al, 1982). For comparison the range of CMB samples formed during high and low flux magmatism are shown in light and dark shaded areas, respectively. Note how the extreme HREE depletion of CMB samples formed during high flux magmatism are comparable to the average CSNB compositions shown, while CMB samples formed during low flux magmatism are not.

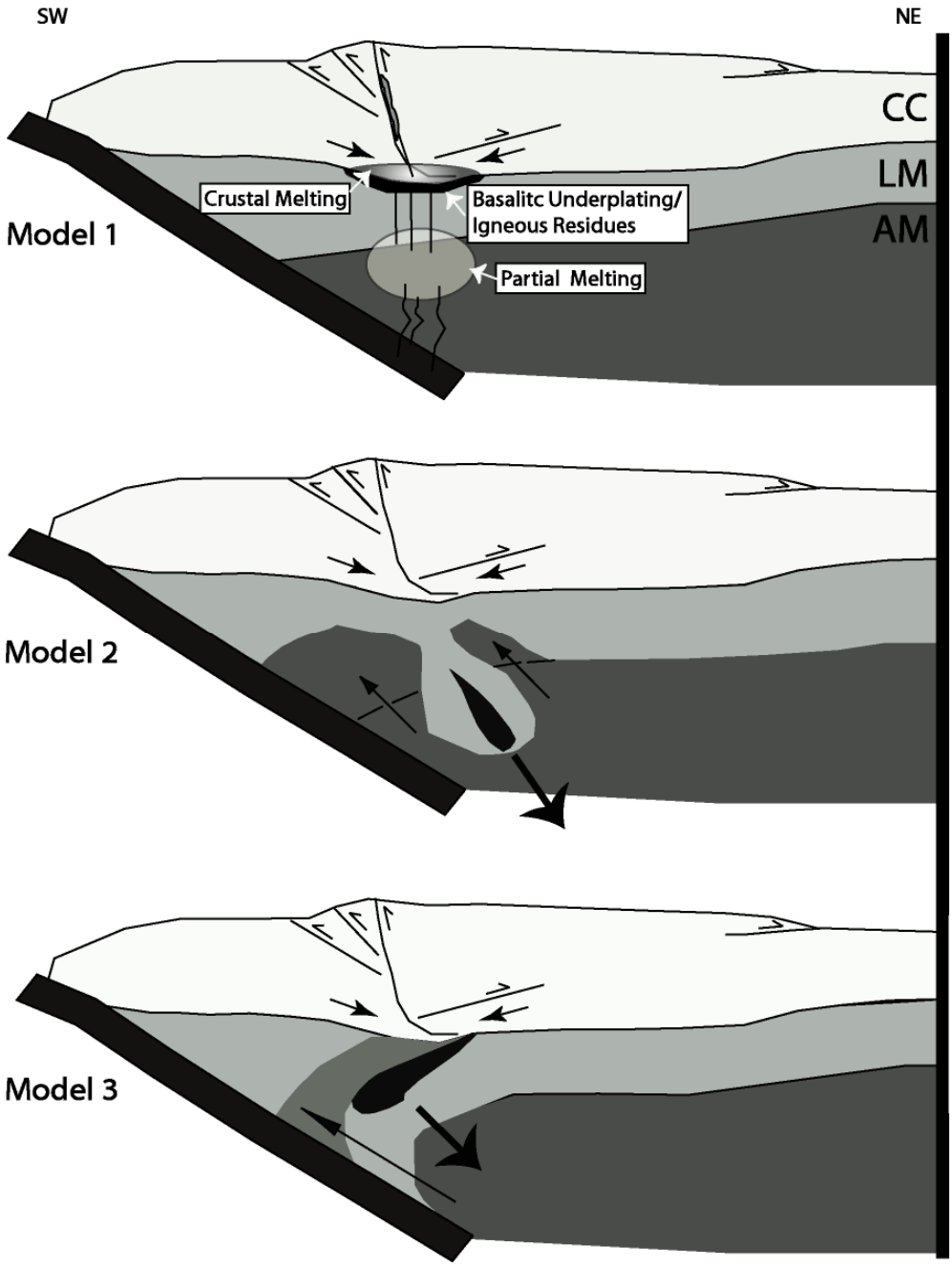

Figure 8: Tectonic models proposed to account for the magmatic flux, isotopic and geochemical trends observed in CMB plutons of this study during 100 – 70 Ma. 1) Trends are driven by deformation in the upperplate; 2) Trends are driven by 1 + a Rayleigh-Taylor instability beneath the upper plate; 3) Trends are driven by 1 + delamination. CC = continental crust, LM = lithospheric mantle, AM = asthenospheric mantle

Table 1. REE, Sm-Nd and Rb-Sr isotopic Data, CMB plutonic rocks

			REE data		Nd Isotopic data				Sr isotopic data		
Sample no.	**Age (T) Ma**	**Age error +/-**	**Eu/Eu***	**$(La/Yb)_N$**	**$^{147}Sm/^{144}Nd$**	**$^{143}Nd/^{144}Nd$ m**	**$\varepsilon_{Nd(T)}$**	**T-DM (Ma)**	**$^{87}Rb/^{86}Sr$**	**$(^{87}Sr/^{86}Sr)m$**	**$(^{87}Sr/^{86}Sr)i$**
Douglas Channel											
GJP-50	152.7	1.9	1.27	3.21					0.0586	0.70469	0.704639
GJP-51	151		0.94	8.37							
GJP-52	149		0.94	11.51					0.1554	0.70419	0.704009
GJP-55	147.8	1.5	1.09	15.91					0.1731	0.703801	0.703673
GJP-56	142.5	1.9	1.09	8.57					0.1285	0.703865	0.703627
GJP-57	146.7	1.7	1.08	37.18	0.127924	0.512785	3.67	483			
GJP-58	144.2	1.5	1.35	21.02	0.145797	0.512837	4.41	493	0.2224	0.704743	0.704482
GJP-60	148.4	1.7	0.77	5.34					0.1816	0.704126	0.703914
GJP-61	148.4	1.7	0.76	4.30	0.12739	0.512785	3.7	480	0.1063	0.70458	0.704437
GJP-62	94.5	1.1	1.07	6.54	0.14138	0.512768	3.21	601	0.1661	0.705032	0.704809
GJP-63	94.5	1.1	0.77	3.93	0.110723	0.512742	3.22	466	0.374	0.705205	0.704632
GJP-64	107.7	1.7	0.83	6.49							
GJP-65	100.9	1.4	0.97	3.94					0.1642	0.704131	0.703904
GJP-67	97	1.1	1.18	4.01	0.118243	0.512689	1.97	583	0.1699	0.704911	0.704677
GJP-68	97	1.1	0.86	7.78	0.16326	0.512519	-1.68	1574	0.0247	0.706189	0.706189
GJP-69	91.9	1.2	1.04	9.73	0.112858	0.512645	1.76	617	0.3743	0.705927	0.705123
GJP-71	82.6	0.9	0.90	8.78	0.122663	0.512715	2.90	567			
GJP-76	188	2.6	0.95	5.68					0.1661	0.70486	0.704511
GJP-83	81.8	1.8	1.01	23.63					0.1765	0.705014	0.704656
GJP-84	60.9	0.8	1.11	6.42					0.1609	0.704886	0.704551
GJP-85	81.9	1.1	0.90	15.65	0.082009	0.51266	2.54	461	0.0922	0.704979	0.70479
GJP-86	81.9	1.1	1.00	5.07	0.134454	0.512777	3.9	534	0.7622	0.705151	0.703543
GJP-89	130.2	1.8	0.90	9.30	0.136011	0.512784	3.99	533	0.2937	0.70455	0.70393
GJP-90	52		1.24	8.01	0.135726	0.512727	3.2	636	0.2775	0.704796	0.704055
MT05-121	NO AGE		1.10	14.42	0.196967	0.512589			0.4313	0.705855	
MT05-128	NO AGE		0.91	2.31	0.113081	0.512831	5.7	349	1.829	0.708408	0.703706
MT05-138	210		0.44	9.96	0.149521	0.512896	6.24	387	0.1969	0.704186	0.703629
MT05-139	NO AGE		0.98	16.30	0.093165	0.512491	-2.17	708	0.2794	0.706117	0.705909
MT05-140	180.8	2.6	0.65	8.11	0.096692	0.512821					
MT05-145	52.3	1.1	0.97	17.56	0.11454	0.512582	-0.55	721	0.2243	0.705898	0.705731
MT05-146	52.4	1.8	1.00	43.17					0.1501	0.705086	0.704399
MT05-149	198.9	3.2	0.82	2.96	0.072146	0.512836			0.0869	0.704233	
MT05-150	NO AGE		0.04	3.55	0.044862	0.51287			0.1857	0.704597	
MT05-155	70.9	1.6	0.97	9.66	0.117589	0.512833	4.52	361	0.2215	0.704348	0.704124

Table 1 (cont.). REE, Sm-Nd and Rb-Sr isotopic Data, CMB plutonic rocks

			REE data		Nd Isotopic data				Sr isotopic data		
Sample no.	**Age (T) Ma**	**Age error +/-**	**Eu/Eu***	**$(La/Yb)_N$**	**$^{147}Sm/^{144}Nd$**	**$^{143}Nd/^{144}Nd$ m**	**$\varepsilon_{Nd(T)}$**	**T-DM (Ma)**	**$^{87}Rb/^{86}Sr$**	**$(^{87}Sr/^{86}Sr)m$**	**$(^{87}Sr/^{86}Sr)i$**
Mathieson Channel											
GJP-43	123.3	1.4	1.07	4.15	0.118042	0.512705	1.88	558	0.2267	0.705196	0.705009
GJP-44	81.7	0.9	0.92	24.13	0.106482	0.512646	0.86	580	0.2989	0.705472	0.705213
GJP-77	55.6	0.7	1.23	32.77					0.1122	0.704522	0.704434
GJP-78	85		0.97	16.64		0.704884			0.1203	0.704985	
GJP-79	59.5	1.7	1.03	10.83					0.1341	0.703712	0.70355
MT05-96	NO AGE		0.91	5.72	0.120758	0.512889	5.8	286	0.0727	0.703805	0.703709
MT05-97	NO AGE		0.31	3.48	0.129107	0.512814		439			
MT05-98	85.1	1.3	0.99	24.74	0.130953	0.512761		541			
MT05-99	87.4	1.6	0.88	17.29	0.145346	0.512741		691	2.3608	0.707787	
MT05-101	NO AGE		1.00	5.35	0.109766	0.512767	3.42	428	0.2738	0.704682	0.704364
MT05-102	85.1	1.3	1.03	9.70	0.142831	0.512837	4.72	474	0.1239	0.704291	0.704073
MT05-106	93	1.7	1.08	13.64	0.127695	0.512826	4.57	413	0.2033	0.704466	0.704169
MT05-112a	102.9	1.5	1.00	5.42	0.132773	0.512825	4.52	438	0.0533	0.704325	0.704253
MT05-113a	105.3	1.6	0.89	3.41	0.129113	0.512788	3.73	485	0.2036	0.704444	0.70414
MT05-114a	94.2	1.4	1.32	11.38	0.112728	0.512742		475	0.0485	0.704455	
MT05-116	NO AGE		0.96	37.72	0.110563	0.512767	3.44	430	0.072	0.704498	0.704412
MT05-117	83.4	1.2	0.99	20.14	0.106678	0.512778	3.72	400			
MT05-135	52.6	1.4	1.67	43.80	0.095352	0.512725	2.38	429	0.3024	0.706993	0.706767
MT05-136	58.2	0.9	0.90	16.07	0.101592	0.512772	3.7	391			
MT05-137	61.1	1.2	0.93	38.33	0.128538	0.512744	2.81	555	0.1268	0.704552	0.704399

Table 1 (cont.). REE, Sm-Nd and Rb-Sr isotopic Data, CMB plutonic rocks

			REE data		Nd Isotopic data				Sr isotopic data		
Sample no.	**Age (T) Ma**	**Age error +/-**	**Eu/Eu***	**$(La/Yb)_N$**	**$^{147}Sm/^{144}Nd$**	**$^{143}Nd/^{144}Nd$ m**	**$\varepsilon_{Nd(T)}$**	**T-DM (Ma)**	**$^{87}Rb/^{86}Sr$**	**$(^{87}Sr/^{86}Sr)m$**	**$(^{87}Sr/^{86}Sr)i$**
Burke/Dean Channels											
GJP-01	144.5	2.9	0.95	4.28	0.126242	0.512856	4.33	357	2.548	0.704469	0.704132
GJP-02	136		1.04	5.12							
GJP-03	72		0.90	18.62	0.111987	0.512873	5.41	285	0.2932	0.704389	0.704169
GJP-04	72		0.52	11.07	0.11644	0.512848	4.64	334	0.2855	0.704408	0.704194
GJP-07	182.4	4.7	0.95	4.25	0.128067	0.512833	4.26	403	0.3053	0.704446	0.704218
GJP-08	68		0.76	7.21					0.2654	0.704645	0.704458
GJP-09	77.3	1.7	0.98	20.53	0.090196	0.512808	4.10	314	0.119	0.704186	0.704088
GJP-10	77		0.49	66.71	0.08763	0.512841	5.32	270	0.1658	0.70432	0.704088
GJP-12	49.5	0.7	0.72	141.94	0.122454	0.512898	5.63	275	0.1375	0.703905	0.703791
GJP-13	98.4	1.8	0.72	157.76	0.109379	0.512948	6.84	174	0.2526	0.703638	0.70338
GJP-14	58.4	1.9	0.93	9.54	0.129054	0.512919	6.11	260	1.6153	0.70543	0.703778
GJP-16	52.7	1.5	1.06	14.13	0.131711	0.512896	5.60	309	0.2401	0.703867	0.703636
GJP-17	9.3	0.4	0.09	7.41	0.128145	0.512894	5.07	301	39.7797	0.709298	0.704158
GJP-18	9.3	0.4	1.06	6.18	0.117064	0.512927	6.43	218	0.2153	0.70371	0.703474
GJP-19	92.1	2.1	0.89	21.14	0.150049	0.512882	5.13	422	0.1747	0.704115	0.703963
GJP-21	52.7	1.5	1.09	15.01	0.142056	0.512911	6.33	321	0.2469	0.703912	0.703404
GJP-22	61.5	1.7	0.95	21.26	0.11924	0.512906	6.58	255	0.2049	0.703758	0.703362
GJP-23	82.8	2.8	0.64	10.02	0.140202	0.512963	7.65	213	0.1381	0.703543	0.703185
GJP-24	157.1	3.2	0.83	11.04	0.124947	0.512907	6.70	268	0.4303	0.704083	0.703122
GJP-27	182.4	4.7	0.84	2.34	0.153952	0.512954	7.16	278	0.2971	0.70418	0.703409
GJP-29	78.8	1.8	0.93	11.36	0.110616	0.512737	2.93	474	0.0915	0.704373	0.704253
GJP-31	9.3	0.4	0.16	5.88	0.126635	0.512934	6.51	229	1.7914	0.70553	0.703422
GJP-32	92.1	2.1	0.93	33.70	0.128213	0.512746	2.80	550	0.0204	0.704264	0.70421
GJP-36	92.0	2.5	1.15	20.33	0.110686	0.512787	3.92	403	0.305	0.704743	0.704344
GJP-37	107.5	1.5	1.09	8.22	0.10115	0.512792	4.12	364	0.1368	0.704422	0.704243
GJP-38	107.5	1.5	1.00	4.63	0.120193	0.512875	5.68	305	0.1576	0.703949	0.703708
GJP-39	107.6	3	0.90	20.17	0.138631	0.512875	5.42	375	0.0907	0.703877	0.703738
GJP-82	49.5	1.5	0.96	2.48	0.112449	0.512816	4.65	366	1.24	0.706074	0.704169